FORMATION OF BREAKING BORES IN FUKUSHIMA PREFECTURE DUE TO THE 2011 TOHOKU TSUNAMI

Shinji Sato[1] and Shohei Ohkuma[2]

Tsunami forces on critical coastal structures were reanalyzed by combining laboratory experiments and numerical tsunami simulation, focusing on the formation of breaking bores and their large force to structures. Laboratory experiments demonstrated that nearshore tsunami is likely to form a breaking bore when the slope of the incident tsunami front is steep and the nearshore bed slope is mild. The impulsive pressure to coastal structures was found to increase with the steepness of the tsunami front. Based on these results, together with numerical simulation of tsunami, the formation of bores was discussed in relation to coastal cliff topography in Fukushima Prefecture.

Keywords: 2011 Tohoku Tsunami, breaking bore, impulsive pressure, coastal structures

INTRODUTION

Many coastal structures were destroyed by the massive Tohoku Tsunami generated on March 11, 2011. Tsunami force exerted to coastal structure must be dependent on the type of structure as well as on the properties of incident tsunami as many studies reported large force generated by breaking bores (*e.g.* Sato and Ohkuma, 2014). In Fukushima Prefecture, tsunami videos taken at Naraha located in the central part of Fukushima showed that the incident tsunami formed a breaking bore before impacting on coastal structures leading to catastrophic damage to coastal communities. However, despite many studies done on the source, type and behavior of tsunami during the last past five years since March 2011, many uncertainties still remain in the nearshore and inland tsunami behaviors, such as dynamics of tsunami-induced flow (Lynett, 2016), sedimentary processes represented by scour, erosion and tsunami deposit (Jaffe et al., 2016), and the interaction with structures (Yeh and Sato, 2016).

In this study, we aimed at understanding the tsunami effect to coastal structures when the tsunami hit as a breaking bore. Laboratory experiments were conducted to understand the formation mechanism of the breaking bores and their large pressure to coastal structures. Based on these results, together with numerical simulation of tsunami, the devastating tsunami damage concentrated to the central part of Fukushima was explained in relation to coastal cliff topography in Fukushima Prefecture.

LABORATORY EXPERIMENTS

Laboratory experiments were conducted in a 32 m long, 0.6 m wide wave flume as shown in **Figure 1**. A hydraulically-driven dam-break gate is installed at 9 m from one end of the flume as shown in **Figure 2**. Steep and mild sloping beds with s=1/7 and 1/29 were placed. Tsunami was generated by abruptly opening the hydraulically-driven gate after raising the water level on the offshore side. The profile of the incident tsunami was controlled by adjusting the water depth h_0 (=0.2 m for s=1/7 and =0.3 m for s=1/29) of the flume, the water level difference Δh (varied from 6 to 24 cm), the speed of the gate operation and the opening of the gate (full or half). The speed of the gate opening was controlled in six steps (1 to 6, 6 denotes the fastest speed) by the oil pressure of the system. The tsunami profile was measured by wave gages installed 1 m from the gate and 0.3 m from the shoreline. We firstly examined the formation of bores. The total number of experimental runs was 17 for s=1/7 and 40 for s=1/29. Then the tsunami pressure to a 6 cm tall seawall situated on the shore was measured for 18 runs with s=1/29. **Table 1** summarizes the condition of all the experiments.

Formation of Breaking Bores

Breaking bores were formed when the front face of the incident tsunami was steep enough. **Figure 3** illustrates a schematic diagram of tsunami profile measured at the offshore wave gage. The height $\Delta\eta$ of the incident tsunami and the time Δt for the water level rise were estimated from the incident tsunami profile measured by the offshore wave gage for every run of experiments. The time Δt was then converted to the horizontal distance Δx by the following equation based on the celerity of long wave:

$$\Delta x = \Delta t \times \sqrt{gh}$$

where h is the average water depth at the tsunami front defined by the following equation:

[1] The University of Tokyo, Civil Engineering Department, 7-3-1, Hongo, Bunkyo-ku, Tokyo, 113-8656 JAPAN
[2] Mitsubishi Cooperation, Tokyo, JAPAN

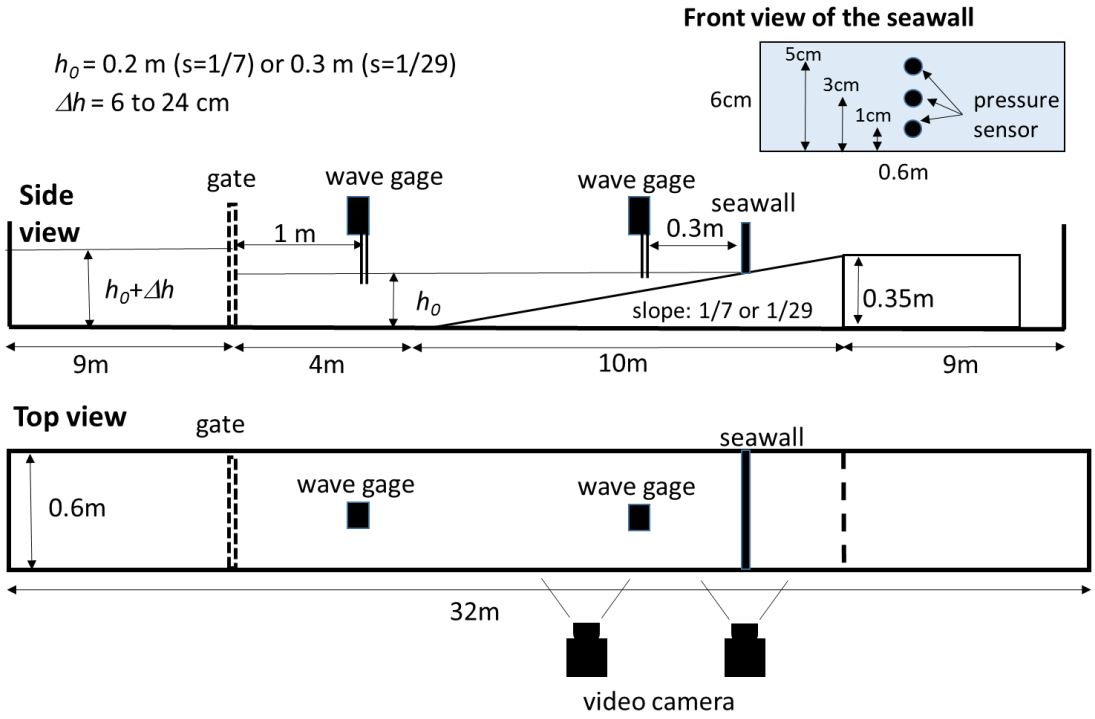

Figure 1. Layout of experiment.

Figure 2. Hydraulically-driven dam-break gate (The speed of the gate can be changed by the oil pressure from 1 (slowest) to 6 (fastest).

Table 1. Conditions of laboratory experiments (Gate speed is from 1 to 6, 1 is the slowest and 6 is the fastest. Gate opening is full (1) or half (1/2).).

(a) bore formation

s=1/7, h_0=0.2 m

$h_0+\Delta h$ (m)	0.38	0.4	0.42	0.44	0.4	0.38	0.4	0.42	0.44
gate speed	5	5	5	5	4	3	3	3	3
gate opening	1	1	1	1	1/2	1/2	1/2	1/2	1/2

s=1/29, h_0=0.3 m

$h_0+\Delta h$ (m)	0.38			0.4			0.42		0.44		
gate speed	5	3	2	5	2	1	5	1	5	2	1
gate opening	1	1/2	1/2	1	1/2	1/2	1	1/2	1	1/2	1/2

$h_0+\Delta h$ (m)	0.46		0.48		0.5		0.52		0.54	
gate speed	5	1	5	1	5	1	5	1	5	1
gate opening	1	1/2	1	1/2	1	1/2	1	1/2	1	1/2

(b) tsunami pressure

s=1/29, h_0=0.3 m

$h_0+\Delta h$ (m)	0.44							0.36	0.38	
gate speed	6	5	4	3	2	1		6	3	
gate opening	1	1	1	1	1	1	1/2	1	1	1/2

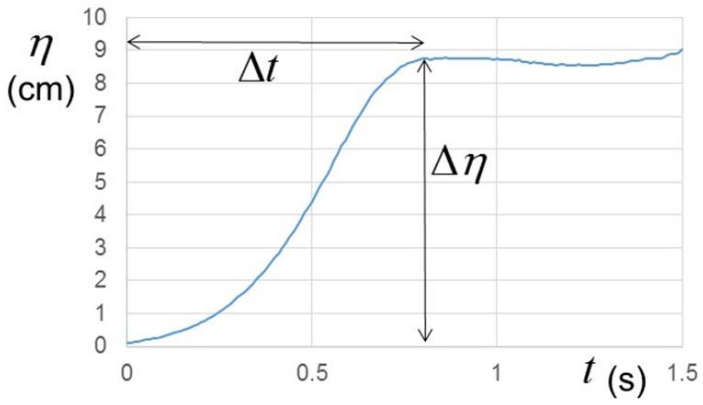

Figure 3. Schematic diagram of incident tsunami.

$$h = h_0 + \frac{\Delta\eta}{2}$$

The spatial slope of the incident wave front $\Delta\eta/\Delta x$ was then estimated for every run of experiment. The still water depth h_b at the breaking point was estimated from the horizontal location of the breaking point identified from the video taken through the glass side wall. **Figure 4(a)** and **4(b)** shows the relationship between the breaker depth normalized by the incident tsunami height $h_b/\Delta\eta$ and the front

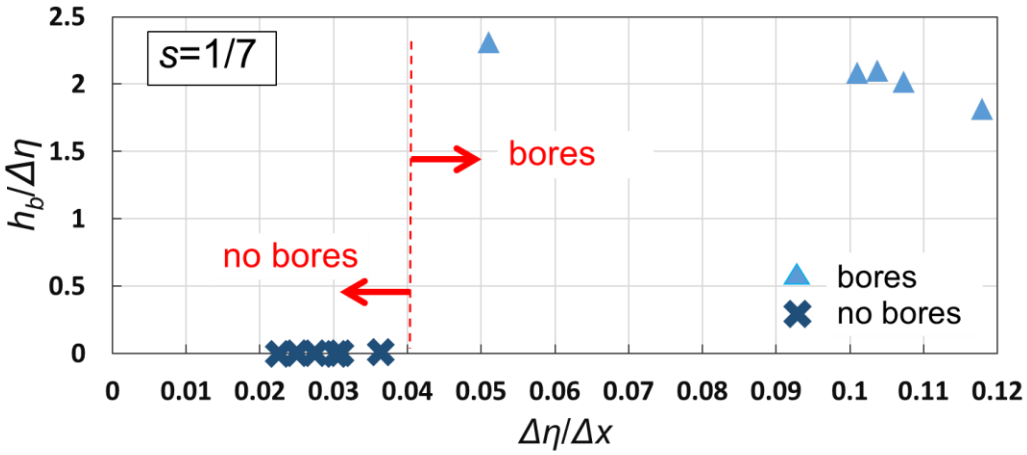

(a) steep slope (s=1/7).

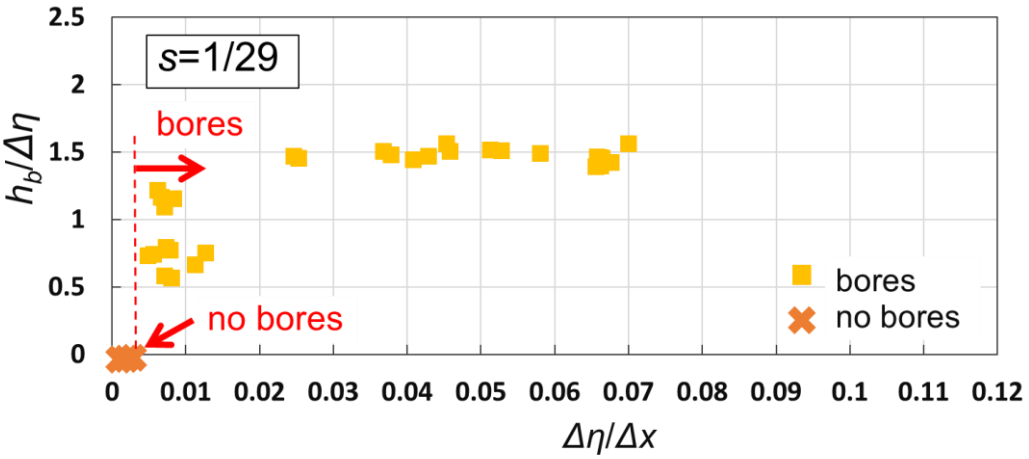

(b) mild slope (s=1/29).

Figure 4. Formation of breaking bore.

slope $\Delta\eta/\Delta x$ of the incident tsunami. Marks 'x' represent for runs in which no breaking bores were formed. For steeper slope (s=1/7, **Figure 4(a)**), bores were observed only on the offshore flat bed. No bores were developed when $\Delta\eta/\Delta x$ < 0.04. On the other hand, for milder slope (s=1/29, **Figure 4(b)**), bores were observed on the slope as well as on the flat bed. The critical wave steepness for the bore formation on the milder slope was $\Delta\eta/\Delta x$ < 0.005, which is one order of magnitude smaller than that for the steeper slope. It is confirmed that the formation of bores is dependent on the slope of incident wave front and that bores are more likely to be formed on milder slope. This is consistent with Goda (1970)'s analysis of periodic wave breaking which demonstrated smaller breaker height for milder slopes.

Pressure to a seawall

A vertical seawall with height 6 cm was situated at the shoreline where tsunami pressure was measured by three pressure sensors installed at z=1, 3 and 5 cm from the bed. The sampling frequency of the pressure was set at 100 Hz since we confirmed the maximum pressure unchanged for higher sampling frequency. **Figure 5** illustrates a series of snapshots of a breaking bore impacting on the seawall for the condition of $h_0+\Delta h$=0.44 m, gate speed 4 and full opening. After the impact (t=0 s), the bore forms a violent splash up to the elevation of 30 cm (t=0.2 s and 0.3 s) before it starts to overflow the seawall (t=0.5 s). The overflow continues for more than 15 s for this case. **Figure 6** illustrates comparisons of incident tsunami profile and water pressure variation recorded at z=1 cm. The gate speed changes from the slowest (1) to the fasted (6). It is noticed that the rising speed of water level increases as the gate speed increases. No breaking bore was formed for the gate speed 1. A breaking bore was formed just in front of the seawall for the gate speed 2. A breaking bore was formed before impacting to the seawall for the gate speed 3, 4, 5 and 6. It is confirmed that the water pressure also

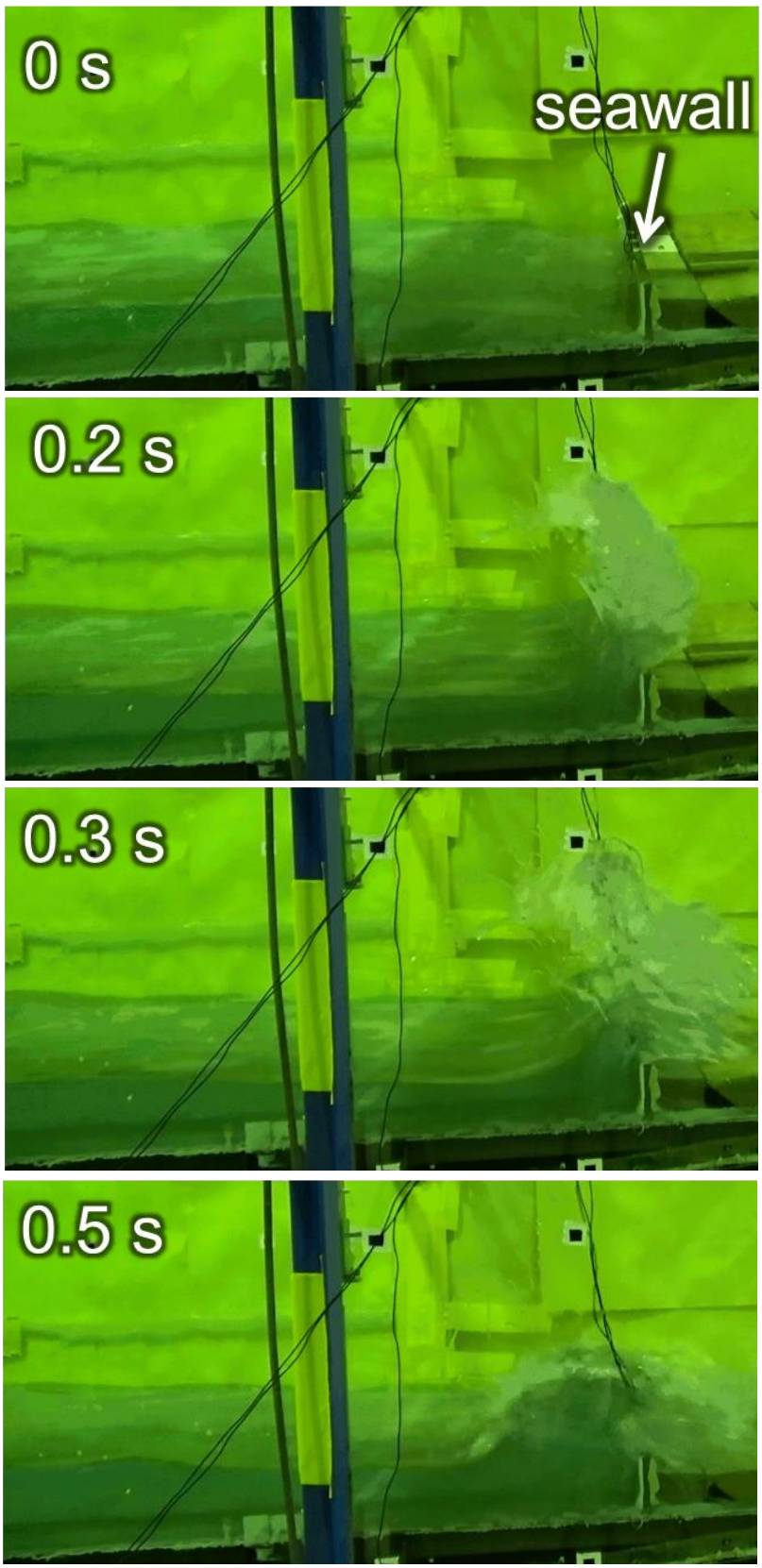

Figure 5. Snapshots of a breaking bore impacting on 6 cm tall seawall (s=1/29, h_0=0.3 m, $h_0+\Delta h$=0.44 m, gate speed=4, gate opening=full).

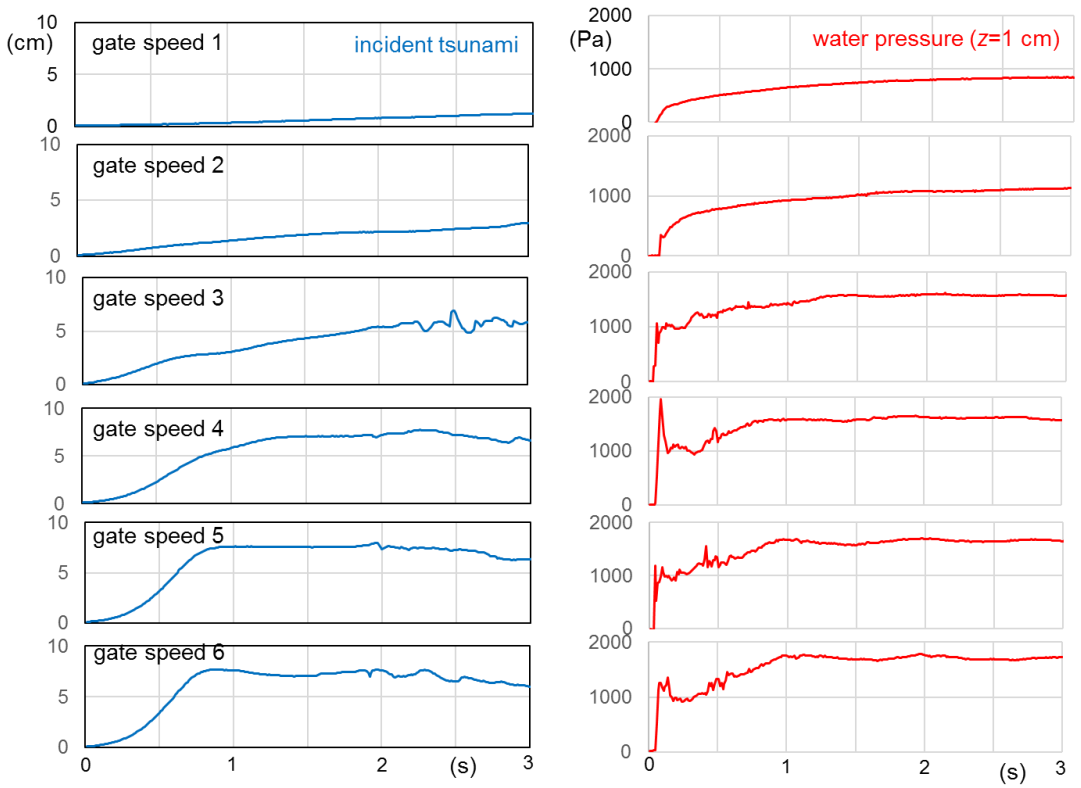

Figure 6. Incident tsunami profile and pressure variation at z=1 cm (s=1/29, h_0=0.3 m, $h_0+\Delta h$=0.44 m, gate opening=full; Note that the time is not synchronized).

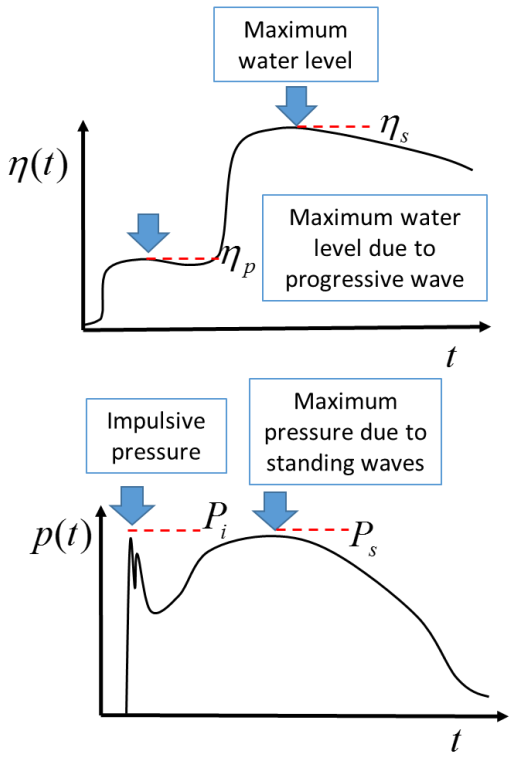

Figure 7. Schematic diagram of tsunami profile in front of the seawall and pressure variation at the seawall due to a breaking bore.

increases as the gate speed increases and forms a sharp peak at the impact in case the bore develops before the impact. **Figure 7** illustrates a schematic diagram of typical tsunami profile and pressure variations observed at the wave gage 0.3 m seaward of the seawall. The pressure is composed of impulsive pressure with a duration of milliseconds and standing wave pressure with several seconds. The impulsive pressure was observed only when the tsunami formed a breaking bore.

Figure 8 shows the relationship between the maximum pressure P_s due to the standing wave and the front slope $\Delta\eta/\Delta x$ of the incident tsunami. The pressure is normalized by the static pressure at the corresponding level due to the maximum water level. It is noticed that the maximum standing pressure is in the range from 1.0 to 1.5 times the corresponding static pressure. No dependency on the front slope is observed. The average standing pressure can be estimated by 1.3 times the corresponding static water pressure.

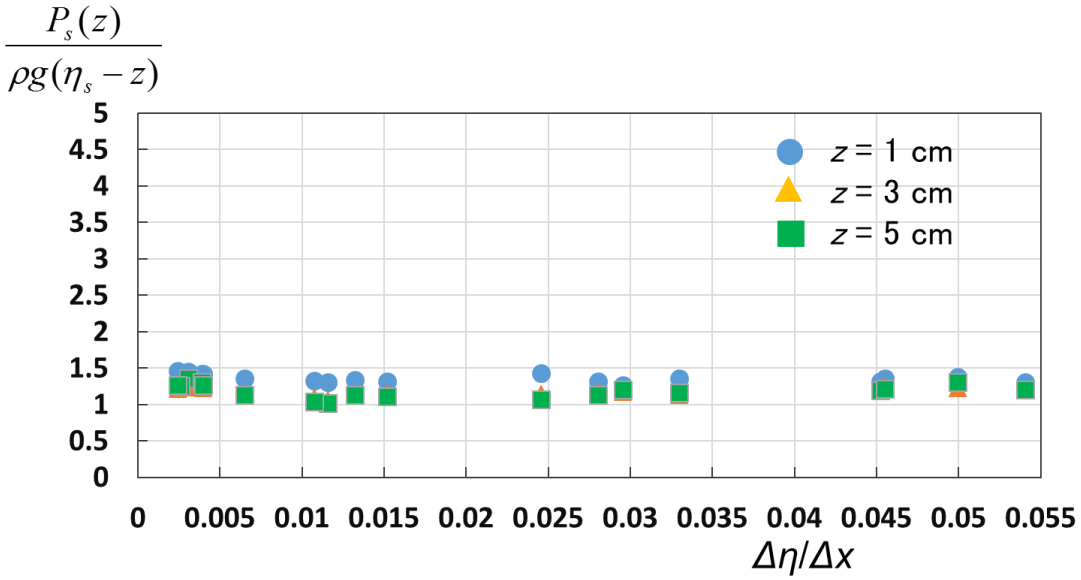

Figure 8. Relationship between the standing pressure $P_s(z)$ and the slope of the incident tsunami.

Figure 9 illustrates the relationship between the maximum impulsive pressure P_i at z=1 cm from the bed and the slope $\Delta\eta/\Delta x$ of wave front. The impulsive pressure is normalized by the static water pressure corresponding to the maximum height of the progressive wave (see **Figure 7**) since Asakura et al. (2000) showed that the maximum impulsive pressure to a vertical wall can be three times as large as the hydrostatic pressure corresponding to the progressive wave. In contrast to the standing pressure, the maximum impulsive pressure was found to increase with $\Delta\eta/\Delta x$ until it reached 3 to 4 times as large as the hydrostatic pressure. The regression analysis yields the relationship expressed by the following equation:

$$\left.\frac{P_i(z)}{\rho g(\eta_p - z)}\right|_{z=1\mathrm{cm}} = 2.1\log_{10}\frac{\Delta\eta}{\Delta x} + 6.2 \qquad (1)$$

which is consistent with Asakura et al. (2000) when the slope of the wave front is in the range from 0.03 to 0.055. The ratio of the maximum impulsive pressure to the hydrostatic pressure decreases when the slope of the wave front is smaller than 0.03. The reason why the impulsive pressure becomes larger for steeper slope of incident wave front appears to be due to the large vertical acceleration developed in steep waves. The dependency of wave steepness on the flow structure in front of the seawall and thus on the large pressure exerted by bores is also confirmed in large-scale flume experiments conducted by Kihara et al. (2015). Such large pressure due to bores is also observed in laboratory experiments by Asakura et al. (2000) and Arikawa et al. (2005). The 2011 Tohoku Tsunami is known to form a breaking bore in the central part of the Fukushima Prefecture as recorded in many videos. Sanuki

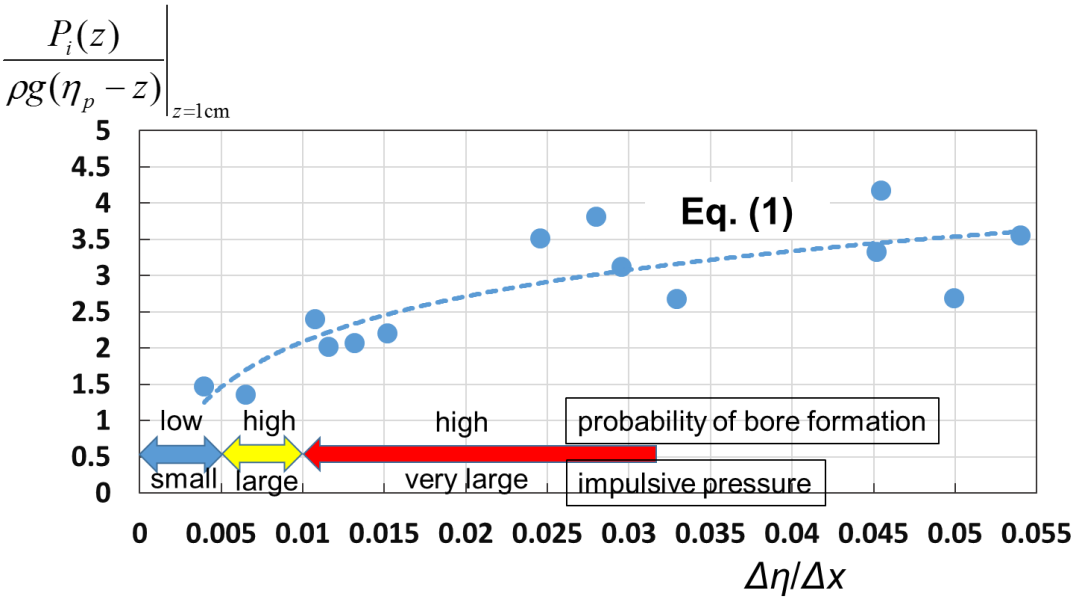

Figure 9. Relationship between the impulsive pressure $P_i(z)$ and the slope of the incident tsunami.

et al. (2013) and Sato and Ohkuma (2014) investigated the massive destruction of seawalls there in relation to the flooding tsunami behavior.

NUMRICAL SIMULATION OF TSUNAMI PROPAGATION IN FUKUSHIMA

Numerical simulation of tsunami propagation was conducted on the basis of the long wave equations. Tsunami source of Satake et al. (2012) was assumed. Tsunami propagation in deep water was calculated by the linear long wave equations in the global coordinate (Sato, 2015). The domain of the computation was from 140 to 146 degrees in the eastern longitude and from 34 to 42 degrees in the northern latitude. The grid size was 0.005 degree and the time step was 1 s. The total duration of the computation was 180 minutes from the earthquake. Nearshore and inland tsunami behavior was computed by the shallow water equation in the Cartesian coordinate in smaller domains situated in 7 nearshore areas. The size of the domains was 20 to 40 km in north to south and 20 to 30 km in east to west. The incident tsunami in the small domain was specified by the offshore tsunami computation. The time step was 0.1 s and the smallest grid size was in the range from 2 m to 10 m. The numerical integration was conducted by the leap frog scheme. No additional mixing term due to breaking wave was introduced. The topography was assumed from the bathymetry data of the Japan Oceanographic Data Center and the high resolution airborne laser profiler data obtained by the Ministry of Land, Infrastructure, Transport and Tourism before the 2011 earthquake.

Figure 10 illustrates the results of the numerical computation in the wide area. **Figure 10(a)** illustrates the bathymetry and **Figure 10(b)** represents the tsunami source proposed by Satake et al. (2012). Although the epicenter of the 2011 Tohoku Earthquake is located in relatively shallow area, a large seafloor deformation is developed near the Japan Trench, where the epicenters of historical tsunami-generating earthquakes are located. After propagating primarily to east and west (**Figure 10(c)**), the tsunami hit the coast in about 30 minutes after the earthquake. **Figure 10(d)** shows a snapshot of tsunami 28 minutes after the earthquake, just before it arrives at Kamaishi in Iwate Prefecture and Onahama in Fukushima Prefecture. Early arrival of tsunami at Onahama in Fukushima appeared to be due to the relatively deep nearshore bathymetry there. It is confirmed that at least three waves approached to the coast in Fukushima Prefecture.

We estimated the slope of the tsunami front from the profile of the surface elevation at 100 m offshore from the shoreline. The slope of the tsunami front was estimated for the largest and the second largest tsunamis by calculating the spatial slope in 40 m east to west horizontal distance. The larger slope was used in the following analysis. The east-west direction represents the cross-shore direction since the tsunami is incident from the east. Then the formation of breaking bores was judged from the

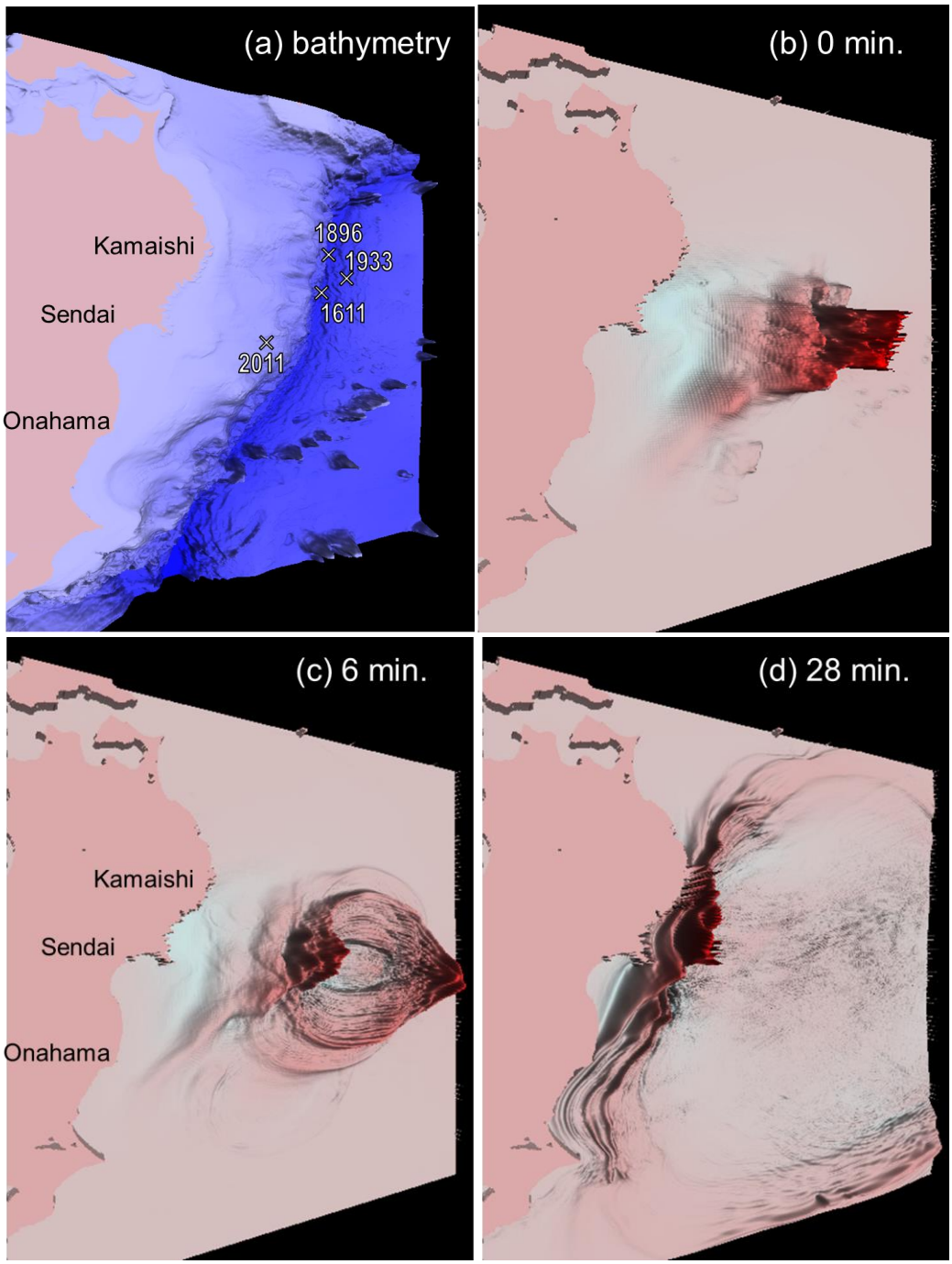

Figure 10. Numerical simulation of the 2011 Tohoku Tsunami in the wide area.

slope of the wave front by using **Figure 4(b)**. The ratio of the maximum impulsive pressure was estimated by using **Eq. (1)**. It is noted however that the laboratory experiments were conducted only with slopes of 1/7 and 1/29 for a single tsunami. In the field, however, the actual bed slope in the nearshore area is about 1/50 and the effect of the preceding tsunami must be considered since the largest tsunami was mostly observed as the second or the third waves. The milder bed slope and the receding flow due to the preceding waves appear to enhance the bore formation. By keeping this in

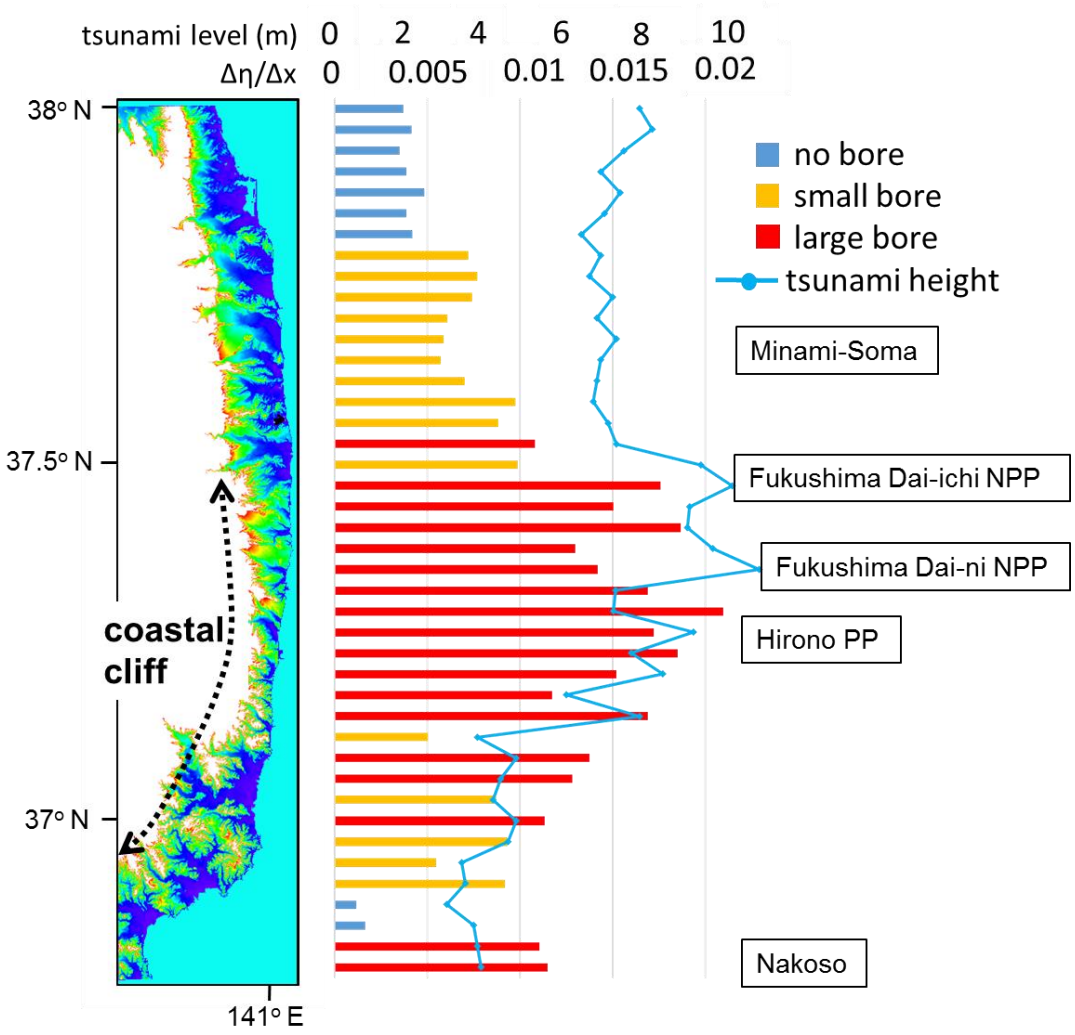

Figure 11. Distributions of the tsunami water level and the slope of wave front in Fukushima Prefecture (The blue line indicates nearshore tsunami level and the bar represents the slope of the tsunami front. Coastal cliff dominates in the central and southern areas specified in the left picture.).

mind, we attempted to classify the effect of bores in terms of $\Delta\eta/\Delta x$ as illustrated in the bottom of **Figure 9**, that is,

the formation of bores is highly probable for $\Delta\eta/\Delta x > 0.005$

and

the maximum impulsive pressure is very large when $\Delta\eta/\Delta x > 0.01$, large for $0.005 < \Delta\eta/\Delta x < 0.01$ and small for $\Delta\eta/\Delta x < 0.005$.

Figure 11 shows the alongshore distributions of the largest tsunami water level (solid blue line) and the slope of the largest wave front (bars). It is noticed that both the tsunami level and the slope of wave front are large in the central part of Fukushima, which is consistent with Sato et al. (2013) which showed the tsunami energy concentrated in the central part of the Fukushima by the offshore bathymetry. The large tsunami height and the steep wave front suggest critical impacts in terms of flooding water level and tsunami force on structures. The slope of the wave front is smaller in the area north to the Fukushima Dai-ichi Nuclear Power Plant although the tsunami level is as large as 7 to 9 m.

In order to understand the difference in tsunami properties observed in **Figure 11**, we investigated the nearshore tsunami behavior in the small computation domain including the Fukushima Dai-ichi Power Plant. **Figure 12** shows the snapshots of tsunami level about 50 minutes after the earthquake when the largest tsunami approached to the domain. Time lag between the two figures is 65 s.

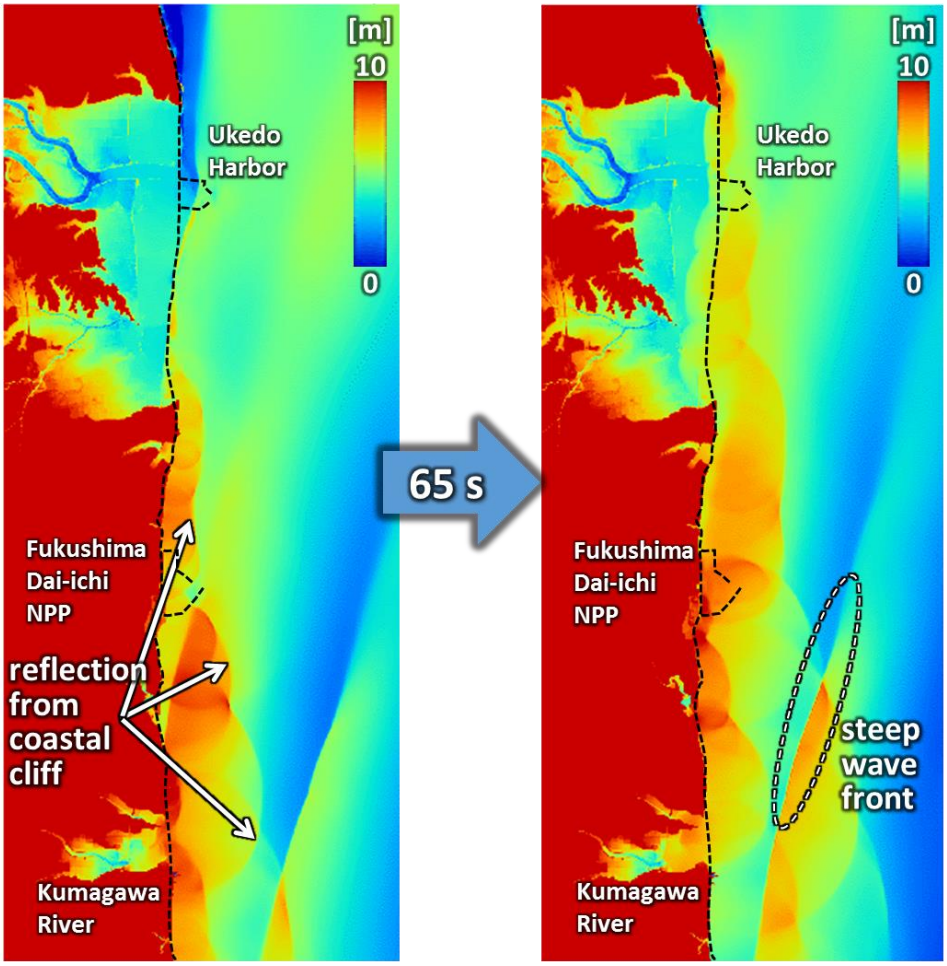

Figure 12. Snapshots of the tsunami water level around the Fukushima Dai-ichi Nuclear Power Plant (about 15:35 pm, March 11, 2011 JST).

Figure 13. Highest watermark in Fukushima observed on the top of a coastal cliff in Tomioka, located between the Fukushima Dai-ichi NPP and the Fukushima Dai-ni NPP (Sato et al., 2013).

Significant tsunami reflection is noticed in the southern area where coastal cliff is dominated (see the left picture of **Figure 11**). The height of the coastal cliff is about 20 to 40 m. **Figure 13** shows a typical example of coastal cliff in Tomioka, located between the Fukushima Dai-ichi NPP and the Fukushima Dai-ni NPP, where the highest watermark in the Fukushima Prefecture is found at 21.1 m above the sea level. On the other hand, in the northern area where a coastal plain with low elevation is dominated, tsunami reflection is insignificant since the preceding tsunami develops flooding into inland. Such difference in the reflection may influence the deformation of the succeeding tsunami to develop steep slope of the wave front.

It is suggested from **Figure 11** and **12** that the formation of the breaking bore as well as the generation of the large impulsive pressure are highly probable in front of the coastal cliff where the slope of the incident tsunami can be increased as a result of the interaction with the reflected tsunami. The influence of the preceding tsunami is also reported by Tadepalli and Synolakis (1994) in which the runup height of the tsunami is increased when the negative tsunami preceded. The large tsunami energy concentrated by the offshore bathymetry and the steep slope of the wave front developed by the interaction with the reflected tsunami from the coastal cliff must have enhanced the formation of the breaking bore and thus increased the tsunami force to coastal structures in the central part of Fukushima.

CONCLUDING REMARKS

Laboratory experiments showed that the angle of the tsunami front was an essential parameter for the generation of breaking bores. Larger impulsive wave force was observed as the angle of the tsunami front became steeper. Numerical simulation revealed that such a steep tsunami was likely to be developed in the central part of Fukushima Prefecture, where the reflection of the preceding tsunami by coastal cliff appeared to enhance the steepness of the largest tsunami. It is therefore important to consider the steepness of the tsunami front in addition to the tsunami height and to pay attention to large impulsive pressure to coastal structures in the areas where breaking bores are likely to be generated.

ACKNOWLEDGMENTS

A part of this study is financially supported by the GRENE Project, Ministry of Education, Culture, Science and Technology, Japanese Government and by the Grant-in-Aid for the Scientific Research provided by the Japan Society for the Promotion of Sciences. The authors appreciate the Ministry of Land, Infrastructure, Transport and Tourism for high resolution topography data and Fukushima Prefecture for assistances to tsunami surveys.

REFERENCES

Asakura R., Iwase K., Ikeya T., Takao M., Kaneto T., Fujii N., and Omori M.: An experimental study on wave force acting on on-shore structures due to overflowing tsunamis. *Proc. of Coastal Engineering*, JSCE, 47, 911-915, 2000 (in Japanese).

Arikawa, T., M. Ikebe, F. Yamada, K. Shimosako and F. Imamura: Large model test of tsunami force on a revetment and on a land structure, *Annual Journal of Coastal Engineering*, JSCE, Vol.52, pp.746-750, 2005 (in Japanese).

Goda, Y.: A synthesis of breaker indices, *Trans. Japan Society of Civil Engineers*, Vol. 2, Part 2, pp. 227-230, 1975.

Jaffe, B., K. Goto, D. Sugawara, G. Gulfenbaum and S. L. Selle: Uncertainties in tsunami sediment transport modeling, *Journal of Disaster Research*, Vol. 11, No. 4, doi: 10.20965/jdr.2016.p0647, pp. 647-661, 2016.

Kihara, N., Niida, Y., Takabatake, D., Kaida, H., Shiba-yama, A. and Miyagawa, Y.: Large-scale experiments on tsunami-induced pressure on a vertical tide wall, *Coastal Engineering*, Vol. 99, pp. 46-63, doi: 10.1016/j.coastaleng. 2015.02.009, 2015.

Lynett, P. J. : Precise prediction of coastal and overland flow dynamics: A grand challenge or a fool's errand, *Journal of Disaster Research*, Vol. 11, No. 4, doi: 10.20965/jdr.2016.p0615, pp. 615-623, 2016.

Sanuki, H., Y. Tajima, H. Yeh and S. Sato.: Dynamics of tsunami flooding to river basin, *Proc.Coastal Dynamics 2013*, Bordeaux, 2013.

Satake, K., Y. Fujii, T. Harada, and Y. Namegaya: Time and space distribution of coseismic slip of the 2011 Tohoku Earthquake as inferred from tsunami waveform data, *Bulletin of the Seismological Society of America*, Vol. 103, No. 2b, doi: 10.1785/0120120122, 2012.

Sato, S., H. Yeh, M. Isobe, K. Mizuhashi, H. Aizawa, H. Ashino: Coastal and nearshore behaviors of the 2011 Tohoku Tsunami along the central Fukushima Coast, *Proc. Coastal Dynamics 2013*, Bordeaux, 2013.

Sato, S. and S. Ohkuma: Destruction mechanism of coastal structures due to the 2011 Tohoku Tsunami in the south of Fukushima, *Coastal Engineering Proceedings*, Vol. 1, No. 34, doi: 10.9753/ice.v34.structures.75, 2014.

Sato, S.: Characteristics of the 2011 Tohoku Tsunami and introduction of two level tsunamis for tsunami disaster mitigation, *Proc. Japan Academy*, Ser. B, Vol. 91, 262-272, 2015.

Tadepalli, S. and Synolakis, C. E.: The run-up of N-waves on sloping beaches, *Proc. Royal Soc. London A*, Vol. 445, pp. 99-112; doi: 10.1098/rspa.1994.0050, 1994.

Yeh, H. and S. Sato: Tsunami effects on buildings and coastal structures, *Journal of Disaster Research*, Vol. 11, No. 4, doi: 10.20965/jdr.2016.p0662, pp. 662-669, 2016.